Presynaptic coupling by electrical synapses coordinates a rhythmic behavior by synchronizing the activities of a neuron pair

Ukjin Choi[a,b], Han Wang[b,1], Mingxi Hu[b], Sungjin Kim[b,2], and Derek Sieburth[b,c,3]

[a]Development, Stem Cell, and Regenerative Medicine Graduate Program, Keck School of Medicine, University of Southern California, Los Angeles, CA 90033; [b]Zilkha Neurogenetic Institute, University of Southern California, Los Angeles, CA 90033; and [c]Department of Physiology and Neuroscience, Keck School of Medicine, University of Southern California, Los Angeles, CA 90033

Edited by Hugo Bellen, Baylor College of Medicine, Houston, TX, and approved April 8, 2021 (received for review November 10, 2020)

Electrical synapses are specialized structures that mediate the flow of electrical currents between neurons and have well known roles in synchronizing the activities of neuronal populations, both by mediating the current transfer from more active to less active neurons and by shunting currents from active neurons to their less active neighbors. However, how these positive and negative functions of electrical synapses are coordinated to shape rhythmic synaptic outputs and behavior is not well understood. Here, using a combination of genetics, behavioral analysis, and live calcium imaging in *Caenorhabditis elegans*, we show that electrical synapses formed by the gap junction protein INX-1/innexin couple the presynaptic terminals of a pair of motor neurons (AVL and DVB) to synchronize their activation in response to a pacemaker signal. Live calcium imaging reveals that *inx-1*/innexin mutations lead to asynchronous activation of AVL and DVB, due, in part, to loss of AVL-mediated activation of DVB by the pacemaker. In addition, loss of *inx-1* leads to the ectopic activation of DVB at inappropriate times during the cycle through the activation of the L-type voltage-gated calcium channel EGL-19. We propose that electrical synapses between AVL and DVB presynaptic terminals function to ensure the precise and robust execution of a specific step in a rhythmic behavior by both synchronizing the activities of presynaptic terminals in response to pacemaker signaling and by inhibiting their activation in between cycles when pacemaker signaling is low.

electrical synapse | innexin | *C. elegans* | lateral excitation | shunting inhibition

Electrical synapses mediate the synchronized firing between neurons that are connected by them (1) and, consequently, play an important role in modulating the strength and timing of synaptic output at chemical synapses (2). Neuronal synchronization by electrical coupling has been widely observed throughout the mammalian central nervous system, including in the cortex (3, 4), inferior olive (5, 6), and retina (7). In addition, the interaction of electrical synapses and chemical synapses can drive neuronal activities more effectively. In cerebellar Golgi cells, electrical synapses between interneurons enhance synchronous activities in response to chemical synaptic inputs (8), and electrically coupled dendrites of the retinal ganglion cells show spike synchrony when chemical synaptic input is integrated (9). Lastly, electrical coupling can enhance downstream chemical synaptic outputs. In the mouse retina electrical synapses between bipolar cells promote glutamate release on retinal ganglion cells (10).

Electrical synapses are composed of multimeric clusters of connexin hemichannels (or innexin channels in invertebrates) that dock with connexin hemichannels on the coupled cell, thereby connecting the cytosols of adjoining neurons, allowing passage of ions and small molecules. One mechanism by which electrical synapses activate coupled neurons is by mediating lateral excitation, whereby an excited neuron drives depolarization of its neighboring neurons through the passage of depolarizing currents through the channel. Lateral excitation mediated by electrical synapses is thought to underlie the ability of electrical synapses to synchronize the activity of neuronal populations and to enhance network activity (2, 11). In mammals, lateral excitation between ON bipolar cells improves sensitivity to motion (10) and between mitral cells in the olfactory bulb amplifies sensory signals (12). In *Caenorhabditis elegans*, electrical coupling between mechanosensory neurons enhances the activities between them through lateral excitation in response to nose touch (13). However, electrical synapses can also inhibit the neuronal activities of coupled neurons as they introduce resistance to the circuit. The inhibition occurs when current leaks from a more depolarized neuron to a less depolarized neuron resulting in the attenuation of the voltage change of the more depolarized neuron. This shunting inhibition can result in a subthreshold depolarization and thereby locally silence neuronal activity at the electrical synapse (11, 14, 15). Shunting inhibition by electrical synapses has been reported in both vertebrate and invertebrate studies. In the retina, simultaneous injection of a subthreshold current pulse into two electrically coupled AII amacrine cells elicits a response, but injection into just one fails to elicit depolarization (7). Striatal interneurons

Significance

Central pattern generators produce rhythmic behaviors that occur on a variety of timescales. Here, using a simple behavioral circuit that repeats every 50 s in *Caenorhabditis elegans*, we show that electrical synapses composed of the gap junction protein INX-1/innexin are necessary for the precise and accurate timing of the behavioral outputs that are controlled by a biological clock. Electrical synapses do so by both promoting synchronized activation of a pair of coupled neurons in response to the signals from the clock and by inhibiting their inappropriate activation when clock signaling is low. Our findings represent one of the first examples of how the execution of a rhythmic behavior is shaped by electrical synapses through coordinating the activities of coupled neurons.

Author contributions: U.C., H.W., and D.S. designed research; U.C., H.W., M.H., and S.K. performed research; U.C., H.W., and M.H. contributed new reagents/analytic tools; U.C. analyzed data; U.C. wrote the paper; and H.W. and D.S. edited the paper.

The authors declare no competing interest.

This article is a PNAS Direct Submission.

[1]Present address: Department of Integrative Biology, University of Wisconsin–Madison, Madison, WI 53706.

[2]Present address: Department of Microbiology and Molecular Biology, College of Bioscience and Biotechnology, Chungnam National University, Daejeon 34134, Republic of Korea.

[3]To whom correspondence may be addressed. Email: sieburth@usc.edu.

This article contains supporting information online at https://www.pnas.org/lookup/suppl/doi:10.1073/pnas.2022599118/-/DCSupplemental.

Published May 10, 2021.

show reduction in firing frequency in response to synaptic inputs, with less correlation due to shunting of currents through electrical synapses (16). In *C. elegans*, the network activity of the hub-and-spoke circuit is suppressed by shunting from an active neuron to an inactive neuron (17), and electrical coupling reduces the activity of a motor neuron that regulates the backward motion through shunting (18). How the excitatory and inhibitory functions of electrical synapses are coordinated to shape the synchronized activity of neurons and how this coordination impacts rhythmic behaviors is not well understood.

The expulsion step of the defecation motor program (DMP) in *C. elegans* is a rhythmic and precisely timed contraction of the enteric muscles that repeats every 50 s and functions to expel contents from the gut (19–21). The circuit that controls the expulsion step consists of the intestine, which functions as the pacemaker, a pair of GABAergic motor neurons, AVL and DVB, and the enteric muscles [Fig. 1*A* (22–25)]. The expulsion step starts with a calcium oscillation in the intestine, which triggers the calcium-dependent secretion of the neuropeptide like protein NLP-40 from dense core vesicles (24–26). Once secreted, NLP-40 binds to AEX-2/G protein–coupled receptor (GPCR) on AVL and DVB motor neurons, leading to their activation by the generation of an all-or-none calcium transient that originates at their neuromuscular junctions (NMJs) (26, 27). Each calcium transient leads to the release of GABA, which functions as an excitatory neurotransmitter to promote contraction of the enteric muscles (23). This excitatory function of GABA, which differs from its classical inhibitory function (28), promotes enteric muscle contraction by activating the GABA-gated cationic channel EXP-1 (23). The expulsion step is highly robust, and its timing is precise, always occurring once 3 s after the start of each cycle (19). It has been proposed that the rhythmic release of NLP-40 from the pacemaker is the instructive signal controlling the timing of AVL and DVB activation. However, NLP-40 is a volume transmitter, diffusing from the intestine to AVL and DVB through a fluid-filled cavity, suggesting that additional mechanisms must exist in AVL/DVB to ensure the robustness and precise timing of their activation.

Here, we demonstrate a role for electrical synapses composed of the gap junction protein INX-1 in functionally coupling the AVL and DVB motor neuron NMJs and in coordinating their activation to control the timing of the enteric muscle contraction. We found that INX-1 synchronizes calcium influx into AVL and DVB by promoting the activation of DVB by AVL in response to pacemaker signaling. In addition, we found that INX-1 inhibits inappropriate activation of the DVB motor neuron during cycle intervals. We propose that the electrical synapses synchronize and amplify synaptic output by promoting lateral excitation in response to pacemaker signaling and inhibit inappropriately timed synaptic activation by shunting inhibition when pacemaker signaling is low.

Results

***inx-1* Regulates the Timing of Expulsion during the DMP** The DMP consists of three sequential muscle contractions that occur every 50 s, beginning with the posterior body wall muscles (pBoc), followed by the anterior body wall muscles (aBoc), and ending with the enteric muscles, which leads to expulsion (Exp) (21, 29). In wild-type animals, expulsion occurs once in every cycle about 3 s after the start of each cycle (as measured by pBoc). Disruption of *nlp-40* signaling does not impact cycle length or pBoc frequency, but expulsion is nearly eliminated, resulting in a reduction of expulsion frequency from 100 to <5% [Fig. 1*B* (22, 26)]. Prior laser ablation studies have shown that AVL or DVB ablation results in an expulsion frequency of 53 or 71%, respectively (22). Prior live calcium imaging studies reveal that a single calcium transient is generated by NLP-40 at the AVL and DVB NMJs every 50 s, and expulsion occurs at the peak of each calcium transient (26). Together, these results suggest a model whereby the rhythmic secretion of NLP-40 from the intestine activates both AVL and DVB, which function in parallel to promote expulsion by calcium-dependent GABA release (Fig. 1*A*).

To investigate the contributions of AVL and DVB on expulsion in more detail, we first genetically ablated AVL or DVB after the expulsion circuit is formed (in the L4 stage), using mini singlet oxygen generator (miniSOG), a genetically encoded photosensitizer that kills neurons by generating reactive oxygen species after blue light illumination (30, 31). To selectively ablate AVL or DVB, we expressed miniSOG under control of a *flp-22* promoter or *flp-10* promoter fragment (32), respectively, and assayed expulsion frequency 24 h after exposure of animals to blue light. As expected, genetic ablation of both AVL and DVB dramatically reduced expulsion frequency to less than 5% (Fig. 1*B*). Genetic ablation of either AVL or DVB reduced the expulsion frequency to 68% and 63%, respectively (Fig. 1*B*), in agreement with the laser ablation studies (22). These results indicate that AVL and DVB contribute roughly equally to contraction of the enteric muscle, but the activation of both neurons is critical for enteric muscle contraction to occur in every cycle.

We next examined the timing of expulsion, and we found that in both wild-type and DVB-ablated animals, expulsion was precisely timed, occurring on average 3 s after the start of each cycle (Fig. 1*C*). However, AVL-ablated animals exhibited a significant delay in the average time of expulsion compared to controls. The majority of expulsions (62%) in AVL-ablated animals occurred at the normal time of 3 s following pBoc (hereafter referred to as normal expulsion), but 38% of expulsions occurred more than 5 s following pBoc (hereafter referred to as ectopic expulsion; Fig. 1 *B* and *C*). As expected, all normally timed expulsions in AVL- or DVB-ablated animals were eliminated by *nlp-40* mutations. However, the ectopic expulsion of AVL-ablated animals were not eliminated by *nlp-40* mutations (Fig. 1 *B* and *C*). These results suggest that in the absence of AVL, DVB can become activated at random times independently of pacemaker signaling.

To determine the molecular mechanism by which ectopic DVB activation occurs, we conducted a forward genetic screen for suppressors that could restore expulsion to *nlp-40* mutants. We identified three suppressors each defining a different gene (*SI Appendix*, Fig. S1*A*). One of the suppressors contained a putative null mutation in *inx-1*, which encodes one of 25 innexin family members in *C. elegans*. Two independently isolated *inx-1* null mutations (*vj46* and *tm3524*; *SI Appendix*, Fig. S1*B*) significantly increased the expulsion frequency of *nlp-40* mutants from <5% to about 40% without altering pBoc frequency or cycle length (Fig. 1*B* and *SI Appendix*, Figs. S1 *A*, *C*, and *D*). Similarly, RNA interference (RNAi)-mediated knockdown of *inx-1* increased the expulsion frequency of *nlp-40* mutants to 37% (Fig. 1*B*). Notably, most of the restored expulsions in *nlp-40*; *inx-1* double mutants were ectopic, occurring more than 5 s after the start of each cycle (Fig. 1 *B* and *C*). *inx-1* single mutants had normal cycle lengths but exhibited a mild reduction in overall expulsion frequency due to both a reduction in normally timed expulsion as well as the occurrence of ectopic expulsion (Fig. 1 *B* and *C* and *SI Appendix*, Fig. S1*C*). NLP-40 also controls the second (aBoc) step of the DMP, and *nlp-40* mutants have significantly reduced aBoc frequency [*SI Appendix*, Fig. S1*D* (26)]. *inx-1* mutations did not suppress the aBoc frequency defects of *nlp-40* mutants (*SI Appendix*, Fig. S1*D*). Thus, *inx-1* has a specific role in negatively regulating the ectopic contraction of the enteric muscles.

***inx-1* Functions in Mature AVL and DVB Motor Neurons to Regulate Expulsion.** To determine in which tissue *inx-1* functions to regulate expulsion, we conducted tissue-specific rescue experiments. Expression of *inx-1* complementary DNA (cDNA) in the GABAergic motor neurons (using the *unc-47* promoter), which includes AVL and DVB, fully reverted the expulsion frequency

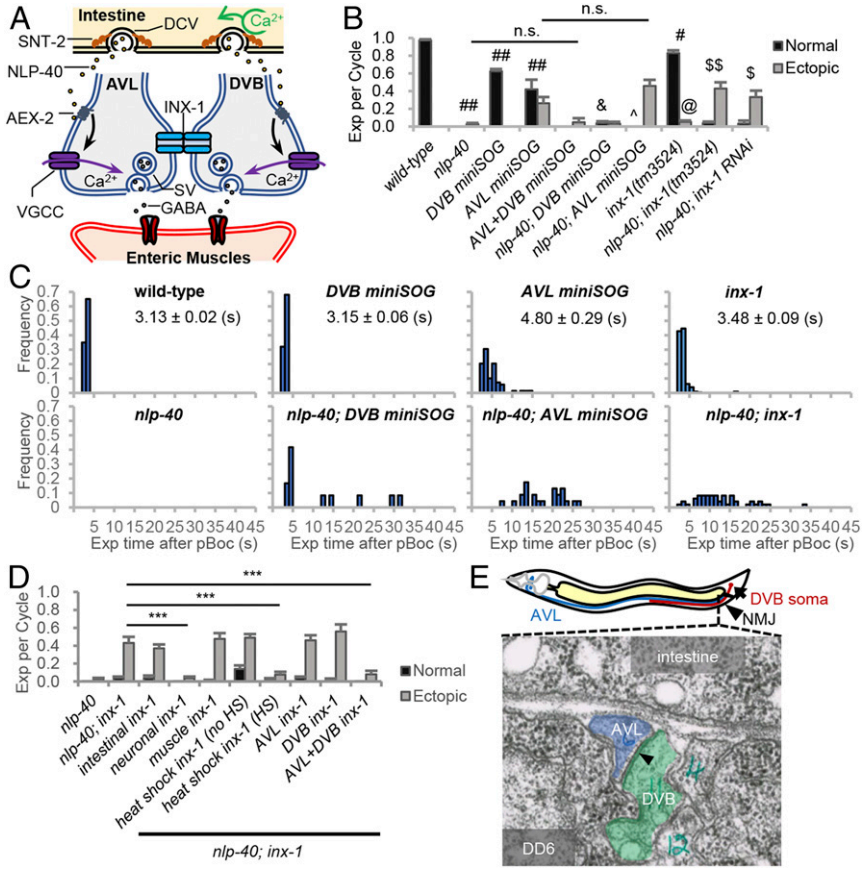

Fig. 1. *inx-1* functions in AVL and DVB motor neurons to regulate the frequency and timing of expulsion during the DMP. (*A*) Model for the circuit regulating expulsion (Exp). Calcium oscillations in the intestine (pacemaker) every 50 s lead to SNT-2/synaptotagmin-dependent secretion of NLP-40 from dense core vesicles (DCVs). NLP-40 activates the GPCR, AEX-2, in AVL and DVB, leading to calcium spike generation through VGCCs and GABA release from NMJs, which leads to the enteric muscle contraction. AVL and DVB NMJs are functionally coupled by INX-1/innexin, which coordinates AVL/DVB activities by suppressing ectopic calcium influx and promoting NLP-40-dependent AVL/DVB activation. (*B*) Quantification of the number of Exp per DMP cycle in adult worms with the indicated genotypes. "Exp per cycle" denotes the ratio of Exp per pBoc, which defines the start of the DMP. "Normal" denotes Exp occurring less than 5 s after pBoc, and "Ectopic" denotes Exp occurring more than 5 s after pBoc. DVB *miniSOG* and AVL *miniSOG* denote transgenes expressing miniSOG under control of a *flp-10* and *flp-22* promoter fragment, respectively. (*C*) Histograms showing the time when each Exp occurred after pBoc in the indicated strains. The average Exp time after pBoc with SEs is shown for wild-type, DVB *miniSOG*, AVL *miniSOG*, and *inx-1* mutants. (*D*) Quantification of the number of Exp per DMP cycle in adult *nlp-40* mutants, *nlp-40; inx-1* mutants or *nlp-40; inx-1* mutants expressing the indicated transgenes. "intestinal *inx-1*" denotes full length *inx-1a* cDNA expressed under the intestine-specific *nlp-40* promoter. "neuronal *inx-1*" denotes *inx-1a* cDNA expressed in GABAergic neurons using the *unc-47* promoter. "muscle *inx-1*" denotes *inx-1a* cDNA expressed in body wall muscles using the *myo-3* promoter. "heat shock *inx-1*" denotes *inx-1a* cDNA expressed using the heat shock promoter (*Phsp-16.2*) either without or with heat shock for 1 h at 34 °C. DVB *inx-1* and AVL *inx-1* denote transgenes expressing *inx-1a* cDNA under control of the *flp-10* and *flp-22* promoter, respectively. (*E*) (*Above*) Diagram showing the cell bodies and axons of AVL/DVB and the NMJ region of AVL/DVB in the preanal ganglia. (*Below*) Transmission electron micrograph image of AVL and DVB axons in cross section in the preanal ganglion region (image JSE_207, also known as JSE_122116), showing a large gap junction (arrowhead) between AVL and DVB axons. The gap junction appears as electron dense areas within the plasma membranes of AVL and DVB where they contact each other. DD6 refers to the soma of the DD6 motor neuron. The electron dense regions of AVL and DVB plasma membranes are present in eight serial sections (JSE_205 to JSE_213). Adapted with permission from David Hall, Albert Einstein College of Medicine. Means and SEs are shown. Student's *t* test: $^{***}P < 0.001$; $^{\#\#}P < 0.001$ compared to wild type; $^{\#}P < 0.01$ compared to wild type; $^{\&}P < 0.001$ compared to DVB *miniSOG*; $^{\wedge}P < 0.01$ compared to AVL *miniSOG*; $^{\$\$}P < 0.001$ compared to *nlp-40*; $^{\$}P < 0.01$ compared to *nlp-40*; $^{@}P < 0.001$ compared to wild type; n.s., not significant.

of *nlp-40; inx-1* mutants from ~50 to 4%. In contrast, expression of *inx-1* cDNA either in the intestine (using the *nlp-40* promoter) or in muscles (using the *myo-3* promoter) failed to revert the expulsion frequency of *nlp-40*; *inx-1* mutants (Fig. 1*D*). *inx-1* cDNA expression in AVL but not DVB or in DVB but not AVL failed to revert the expulsion frequency of *nlp-40; inx-1* mutants. However, coexpression of *inx-1* cDNA in both AVL and DVB fully reverted the expulsion frequency of *nlp-40; inx-1* to 8% (Fig. 1*D*). Thus, *inx-1* is required simultaneously in AVL and DVB to negatively regulate ectopic expulsion.

AVL and DVB are integrated into the motor circuit postembryonically following the first larval stage (21, 33). To determine whether *inx-1* regulates AVL and DVB development or function, we expressed *inx-1* cDNA in adults using a heat shock promoter fragment [from *hsp-16.2* (34)]. Heat shock of transgenic *nlp-40*; *inx-1* adults for 1 h reverted their expulsion frequency to 10% (Fig. 1*D*), indicating that *inx-1* expression after development of the circuit is sufficient to rescue *inx-1* mutants. In support of a postdevelopmental role for INX-1, *inx-1* adults did not exhibit obvious differences in AVL or DVB morphology or in presynaptic vesicle pools sizes at NMJs compared to wild-type controls (*SI Appendix*, Fig. S1*E*). Together, these results indicate that *inx-1* regulates the function of mature AVL and DVB NMJs.

INX-1 Is Concentrated at AVL/DVB NMJs, Where It Functions to Regulate Expulsion Frequency. AVL and DVB each extend a single process along the ventral nerve cord to the preanal ganglion,

where they form en passant NMJs with the enteric muscles (Fig. 1*E* and ref. 35). Examination of serial electron micrographs used to determine the wiring diagram of the nervous system reveal that AVL and DVB processes are often opposed to each other in the preanal ganglion and that they are connected by at least one large gap junction that extends for several sections and lies in close proximity to their NMJs (Fig. 1*E* and ref. 35). To determine whether INX-1 might be a component of this gap junction, we examined the localization pattern of fluorescent INX-1 fusion proteins in AVL and DVB. *inx-1* encodes two isoforms, INX-1A and INX-1B, which have unique C-terminal intracellular tails that arise by alternative splicing (*SI Appendix*, Fig. S2*A*). Expression of either INX-1A::GFP or INX-1B::GFP fusion proteins in GABAergic motor neurons fully reverted the expulsion frequency of *nlp-40; inx-1* mutants to 5% (*SI Appendix*, Fig. S2*A*), indicating that both isoforms are functional and that their localization pattern should reflect that of endogenous INX-1. Both INX-1A::GFP and INX-1B::GFP localized to AVL and DVB somas as well as to one or two puncta located in the preanal ganglion that colocalized with the presynaptic active zone marker UNC-10/RIM1a::mCherry (Fig. 2*A* and *SI Appendix*, Fig. S2D and ref. 36). We identified a 16-amino-acid region (from aa 356 to 372) in the INX-1 intracellular C-terminal domain, that is necessary for both INX-1::GFP's localization to NMJs and for reversion of the expulsion phenotype of *nlp-40; inx-1* mutants (*SI Appendix*, Fig. S2 *B–D*). Thus, INX-1 is highly concentrated at AVL and DVB NMJs, and its localization to NMJs, which is mediated by its cytoplasmic tail, strictly correlates with its ability to regulate expulsion.

INX-1 Functions as a Gap Junction Protein to Couple AVL and DVB Motor Neurons. Several lines of evidence point to a role for INX-1 as a gap junction protein that functionally couples AVL and DVB NMJs during expulsion. First, INX-1::GFP fusion proteins expressed selectively in AVL accumulated at one or two puncta at the preanal ganglion, which colocalized with puncta of INX-1::mCherry expressed in DVB (Fig. 2*B* and *SI Appendix*, Fig. S3*A*). Second, genetic manipulations that disrupt the association of AVL and DVB NMJs suppressed the expulsion defects of *nlp-40* mutants to a similar extent as *inx-1* mutations. *unc-33* encodes a collapsin response mediator protein ortholog essential for axon outgrowth (37, 38). In *unc-33* mutants, the AVL process terminated prematurely before reaching the preanal ganglion (*SI Appendix*, Fig. S3*B*), and the expulsion frequency was 44%, similar to the expulsion frequency in animals in which AVL is ablated (Fig. 1*B* and ref. 22), suggesting a failure of AVL to form NMJs with enteric muscle. Importantly, *unc-33* mutations suppressed the expulsion defects of *nlp-40* mutants to 47%, and the suppression was reverted by expressing *unc-33c* cDNA in GABAergic motor neurons (Fig. 2*D*). Finally, in mammals, connexins can form gap junctions, whereas pannexins only form channels (39–41). Expression of the mammalian pannexin, PANX1, in GABAergic neurons failed to revert the expulsion frequency of *nlp-40; inx-1* mutants (Fig. 2*E*), whereas expression of mammalian connexin, Cx36 (42), which colocalized with INX-1 at AVL and DVB NMJs (Fig. 2*C*), completely reverted the expulsion frequency of *nlp-40; inx-1* mutants to 5% (Fig. 2*E*). Although we have not ruled out that the failure of PANX1 to rescue was due to lack of efficient expression, altogether these results suggest that INX-1 functions as a gap junction protein at AVL and DVB NMJs to regulate expulsion.

Gap junctions can assemble into heteromeric, heterotypic, and homotypic complexes (43). To determine whether *inx-1* might function with other innexins to regulate expulsion, we knocked down (by mutation or by RNAi) each of the other 24 innexins encoded by *C. elegans*. Only knockdown of *inx-1* but not any of the other innexins significantly increased expulsion frequency in

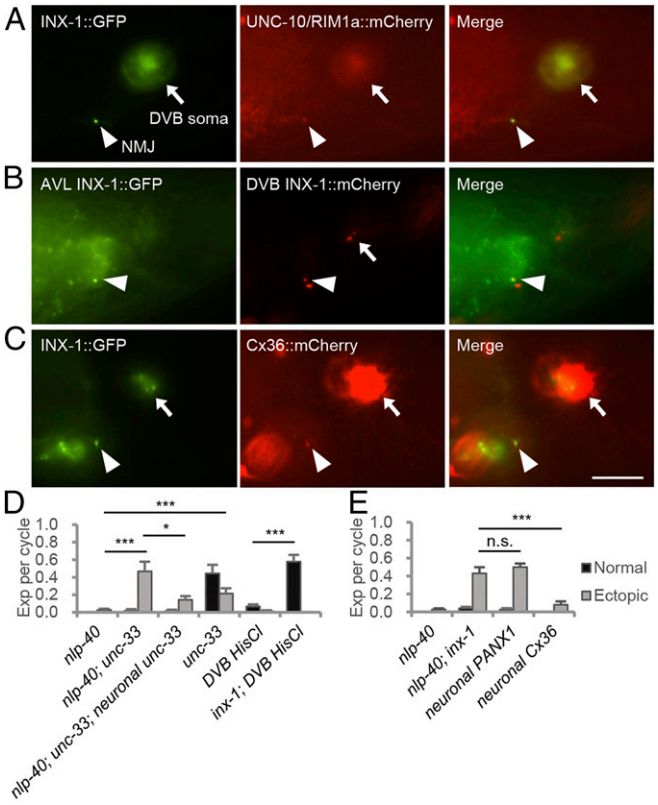

Fig. 2. INX-1 is a gap junction protein that functionally couples AVL and DVB motor neurons at NMJs. (*A*) Representative images of AVL/DVB NMJs (arrowhead) and DVB soma (arrow) from young adults coexpressing INX-1::GFP and UNC-10/RIM1::mCherry fusion proteins in GABAergic motor neurons (AVL and DVB) under the *unc-47* promoter. (*B*) Representative images of AVL/DVB NMJs (arrowhead) and DVB soma (arrow) from young adults coexpressing INX-1::GFP in AVL (under the *unc-25(Δ)* promoter) and INX-1::mCherry in DVB (under the *flp-10* promoter). (*C*) Representative images of AVL/DVB NMJs (arrowhead) and DVB somas (arrow) from young adults coexpressing INX-1::GFP and mouse Cx36::mCherry fusion proteins under the *unc-47* promoter. (*D*) Quantification of the number of Exp per defecation cycle in adults with the indicated genotypes. *unc-33*c cDNA was expressed under the GABAergic neuron-specific (*Punc-47*) promoter. "DVB HisCl" denotes expressing HisCl1 under the *flp-10* promotor. (*E*) Quantification of the number of Exp per defecation cycle in adults with the indicated genotypes. Human PANX1 cDNA and synthetic/mouse Cx36 gene were expressed under the GABAergic neuron-specific (*Punc-47*) promoter. (Scale bar, 10 μm.) Asterisks indicate significant differences: ***$P < 0.001$ and *$P < 0.05$ in Student's *t* test; n.s., not significant.

nlp-40 mutants (*SI Appendix*, Fig. S4), suggesting that INX-1 may function as a homotypic gap junction at AVL and DVB NMJs.

INX-1 Functionally Couples AVL and DVB NMJs during the DMP. To further test the importance of INX-1 in coupling AVL and DVB NMJs, we used the histamine activated chloride channel, HisCl1, whose activation by acute histamine exposure silences neurons by promoting chloride influx through the channel and neuronal hyperpolarization (44). We reasoned that if AVL and DVB are coupled by gap junctions, then silencing one neuron using HisCl1 should also silence the other neuron since chloride ions should pass between them, leading to the elimination of expulsion. On the other hand, if AVL and DVB are not coupled by gap junctions, then inactivation of one neuron by HisCl1 should mimic the effects of ablation of that neuron and reduce expulsion frequency to about 60% (Fig. 1*B* and ref. 22). We found that 30 min histamine treatment of animals expressing HisCl1 in DVB nearly eliminated expulsion in wild-type animals. However, HisCl1 activation failed

to eliminate expulsion in *inx-1* mutants. Instead, expulsion frequency was reduced to 60% (Fig. 2*D*). Thus, HisCl1 activation in DVB can silence both AVL and DVB by passing chloride ions through INX-1. Together these results indicate that AVL and DVB NMJs are functionally coupled by INX-1.

INX-1 Synchronizes the Activation of AVL and DVB by NLP-40. To determine whether *inx-1* functions to synchronize the activation of AVL and DVB, we conducted live fluorescence imaging of animals expressing the genetically encoded calcium sensor GCaMP in AVL and DVB. Since the AVL and DVB NMJs overlap, we distinguished between AVL and DVB activation by quantifying GCaMP fluorescence at the AVL axon tip and the DVB soma, which occupy distinct areas just posterior of the NMJs (Fig. 3*A*). The calcium spikes in AVL activate the entire neuron, whereas the calcium spikes in DVB originate at the NMJ and spread along the axon, reaching the DVB soma within 500 ms (Movies S1 and S2 and ref. 45). In wild-type animals, both AVL and DVB were inactive in between expulsions, and each neuron exhibited a single calcium spike within 500 ms of the other neuron after the start of each cycle (measured by pBoc, n = 29 cycles; Fig. 3 *A*–*D* and Movie S1). In *inx-1* mutants, AVL and DVB activation was largely asynchronous, with calcium spikes occurring within 500 ms of each other in just 33% of the cycles (n = 12 cycles), with DVB activation occurring greater than 500 ms after AVL in 55% of the cycles (n = 20 cycles), and AVL activation occurring more than 500 ms after DVB activation in 11% of the cycles (n = 4 cycles). When AVL activated first, the delay in DVB activation ranged from more than 500 ms to 15 s after AVL activation, and when DVB activated first, the delay in AVL activation ranged from more than 500 ms to 4 s (Fig. 3 *C* and *D* and Movie S2). In *inx-1* mutants, during cycles with synchronized firing, expulsion was always observed at the peak of the AVL/DVB calcium spikes as seen in wild type (Fig. 3*E*). However, during cycles with asynchronous firing, expulsion was observed either at the peak of the calcium spike of the first neuron or second neuron with equal frequency, and in about 10% of cycles, expulsion was all together absent (Fig. 3*E*). Together, these results reveal that the coupling of AVL and DVB NMJs by INX-1 is critical for synchronizing AVL and DVB activation. Moreover, the observation that asynchronous AVL and DVB activation is occasionally associated with missing expulsion suggests that activation of both neurons is necessary to ensure sufficient GABA is released to trigger enteric muscle contraction.

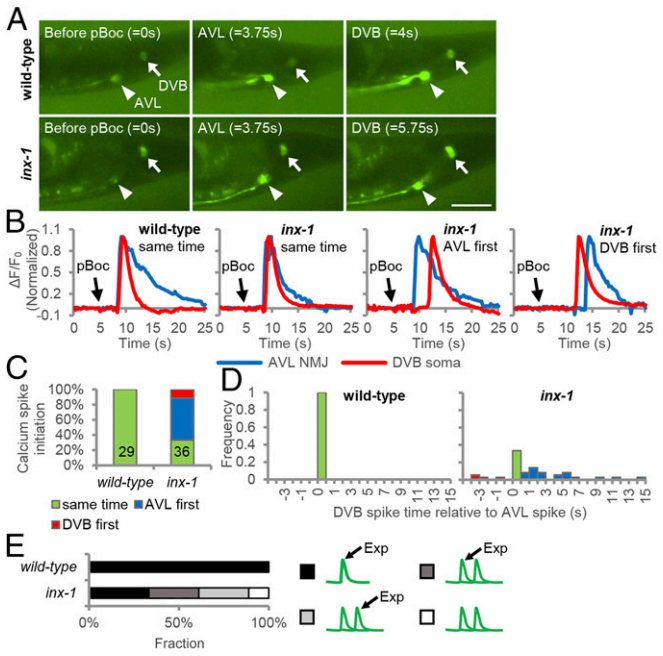

Fig. 3. INX-1 synchronizes the activation of AVL and DVB motor neurons. (*A*) Representative images from videos showing GCaMP fluorescence in the AVL NMJ (arrowhead) and the DVB soma (arrow) before pBoc, at AVL activation onset, and at DVB activation onset in animals expressing GCaMP3 in DVB [under the *unc-47(mini)* promoter] and GCaMP6 in AVL (under the *nmur-3* promoter). (Scale bar, 20 μm.) (*B*) Representative normalized traces showing the calcium dynamics at the AVL axon tip and DVB cell body during the defecation cycle in adult animals with the indicated genotypes. "same" denotes where the calcium spike in DVB cell body initiates within 500 ms after the calcium spike in AVL NMJ initiates; "AVL first" denotes where the calcium spike in DVB cell body initiates more than 500 ms after the calcium spike in AVL NMJ initiates, and "DVB first" denotes where the start of the calcium spike in DVB cell body precedes the start of calcium spike in AVL NMJ. (*C*) Calcium spike initiation time is quantified with the indicated genotypes. (*D*) Histogram showing the initiation time of each calcium spike in DVB cell body relative to the initiation of calcium spike in AVL NMJ with the indicated genotypes. (*E*) The frequency with which Exp occurs at the first or second spike is quantified for the indicated genotypes.

Activation of AVL by NLP-40 Can Elicit Calcium Spikes in DVB through INX-1. To determine whether INX-1 promotes synchronization of AVL and DVB activation by a lateral excitation mechanism, we examined whether AVL could activate DVB. AEX-2 is the NLP-40 GPCR that functions in AVL and DVB to promote expulsion, and *aex-2* mutants have <5% expulsion frequency (27). We generated transgenic animals in which only AVL but not DVB could respond to endogenous NLP-40 by expressing *aex-2* cDNA selectively in AVL in *aex-2* mutants (Fig. 4*A*). As expected, the expulsion frequency in these animals was 48% (Fig. 4*B*), which is similar to the expulsion frequency of DVB-ablated animals (Fig. 1*B*). Live imaging of GCaMP in DVB of these animals revealed that each expulsion was invariably accompanied by a calcium spike at the DVB NMJ (Fig. 4*C* and Movie S3). These results show that in the absence of pacemaker input to DVB, DVB can nevertheless be activated in response to pacemaker signaling. Because AVL is activated in every cycle (Fig. 3), these results indicate that DVB is laterally excited by depolarizing currents generated at the AVL NMJ by NLP-40.

inx-1 mutations further reduced the expulsion frequency of the DVB-silenced animals from 48 to 22% (Fig. 4*B*) and eliminated calcium spikes in DVB in 50% of the cycles (n = 22 cycles) in which expulsion occurred (Fig. 4*C* and Movie S4). Thus, the activation of AVL by the pacemaker signal leads to activation of DVB that depends, in part, on INX-1. These results suggest that INX-1 synchronizes AVL and DVB activity and GABA release in response to NLP-40 through a lateral excitation mechanism.

INX-1 Inhibits Ectopic Calcium Spike Generation at the DVB NMJ. Since *inx-1* mutants exhibit ectopic enteric muscle contractions, we reasoned that electrical synapses composed of INX-1 may also function to inhibit AVL and DVB activity in between cycles via a shunting mechanism. To test this idea, we conducted live calcium imaging of wild-type or *inx-1* mutants expressing GCaMP selectively in DVB. Both wild-type and *inx-1* mutants exhibited a single calcium spike after each pBoc that were similar in amplitude and duration (*SI Appendix*, Fig. S5 *A* and *B*) and were eliminated in *nlp-40* mutants (Fig. 5 *C* and *D*). However, *inx-1* mutants exhibited at least one additional ectopic calcium spike in 50% of the cycles that occurred at random times during the 50 s interval in between cycles (Fig. 5 *A* and *B*) that, on average, was similar in duration but decreased in amplitude, compared to wild-type calcium spikes (*SI Appendix*, Fig. S5*A*). *nlp-40* mutants exhibit no calcium spikes in DVB in any cycle (Fig. 5 *C* and *D* and ref. 26). *nlp-40; inx-1* double mutants lacked normally timed calcium spikes, but still exhibited at least one ectopic calcium spike in each cycle that occurred at random times (Fig. 5 *C* and *D*), that was similar in average amplitude and duration to the calcium spikes of wild-type controls

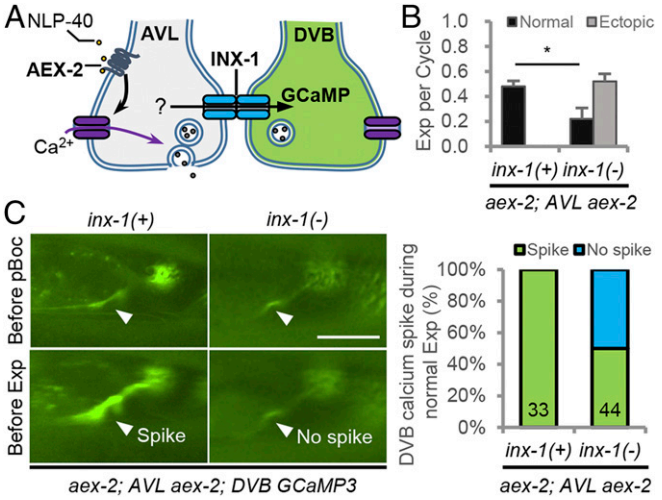

Fig. 4. INX-1 promotes expulsion and DVB activation by AVL in response to pacemaker. (*A*) Schematic showing the strategy used to monitor DVB activation in the absence of pacemaker signaling. The NLP-40 receptor *aex-2* was expressed only in the AVL motor neuron (under the *flp-22* promoter), and the calcium indicator GCaMP3 was expressed in the DVB motor neuron (under the *flp-10* promoter) in *aex-2* mutants. (Scale bar, 20 μm.) (*B*) Quantification of the number of Exp per defecation cycle in adults with the indicated genotypes. "*aex-2; AVL aex-2*" denotes *aex-2* cDNA expressed in AVL in *aex-2* mutants. (*C*, *Left*) Representative images from a real time video showing GCaMP3 fluorescence in the NMJ (arrowhead) either right before the pBoc or the Exp step. (Scale bar, 20 μm.) (*C*, *Right*) Quantification of the number of calcium spikes observed during normal Exp. Means and SEs are shown. Asterisks indicate significant differences: $*P < 0.05$ in Student's *t* test.

(*SI Appendix*, Fig. S5*B*). These results indicate that INX-1 functions to inhibit muscle contractions in between cycles by preventing the generation of ectopic calcium spikes at DVB (and likely also AVL) NMJs. We conclude that DVB can be spontaneously active in between cycles but this activity is inhibited via the shunting of current generated in DVB to AVL through INX-1.

Suppression of Ectopic Calcium Influx by INX-1 Occurs through Inhibition of EGL-19 Voltage-Gated Calcium Channels. To determine the molecular mechanism by which INX-1 inhibits the ectopic activation of AVL and DVB, we examined genetic interactions between *inx-1* and components of the signaling cascade that activates AVL and DVB. *snt-2* encodes a synaptotagmin family member that positively regulates NLP-40 secretion from the intestine, and *snt-2* mutants exhibit reduced expulsion frequency compared to wild-type controls (Figs. 1 *A* and *B* and ref. 26). *inx-1* mutations increased the expulsion frequency of *snt-2* mutants from 55 to nearly 80% (Fig. 6*B*). AEX-2/GPCR binding by NLP-40 activates AVL/DVB through a signaling cascade composed of the heterotrimeric G protein GSA-1/Gαs, adenylate cyclase, and KIN-1/Protein kinase A (Fig. 6*A*). Knockout or knockdown of any of these signaling components nearly eliminates expulsion (26, 27, 45). *inx-1* mutations significantly increased expulsion frequency (to about 40%) in animals compromised in any of these signaling components, and the restored expulsions were nearly exclusively ectopic (Fig. 6*B*). Thus, INX-1 functions independently of the NLP-40–PKA signaling pathway in AVL and DVB to suppress their activation in between cycles.

Calcium influx into the DVB NMJ in response to NLP-40–PKA signaling is mediated primarily through *egl-19*, an L-type voltage-gated calcium channel (VGCC), and *unc-2*, a non-L-type VGCC (45). We found that *egl-19*/VGCC mutations completely abolished the ectopic expulsions associated with *inx-1 aex-2* double mutants (Fig. 6*B*). In addition, *egl-19*/VGCC mutations significantly reduced the ectopic calcium spikes in DVB of *inx-1* mutants (Fig. 6*C*). In contrast, *unc-2*/VGCC mutations had no significant effect on ectopic expulsion frequency of *nlp-40; inx-1* double mutants or ectopic calcium spike frequency of *inx-1* mutants (Fig. 6 *B* and *C*). Together, these results indicate that the activity of the *egl-19* VGCC drives ectopic calcium spike generation in the absence of pacemaker signaling.

To determine whether the ectopic calcium spike generation through EGL-19 is voltage regulated, we examined *egl-36* mutants. *egl-36* encodes a shaw-type voltage-gated potassium channel that is expressed in AVL and DVB (46). *egl-36(n2332)* loss-of-function mutants exhibited normal expulsion frequency (Fig. 6*D*), whereas *egl-36(n728)* gain-of-function mutants, which have hyperpolarized neuronal membranes (46), exhibited 35% expulsion frequency (Fig. 6*D*). Transgenic animals over-expressing *egl-36(gf)* cDNA selectively in GABAergic neurons, exhibited more severe expulsion frequency defects compared to the *egl-36(gf)* mutants (Fig. 6 *D* and *E*), indicating that the *egl-36* potassium channel functions cell-autonomously to decrease AVL and DVB excitability in a dose-dependent manner. Expression of constitutively active PKA in AVL and DVB restores enteric muscle contractions to *nlp-40* mutants (45) but failed to restore expulsion to *egl-36(gf)* mutants (Fig. 6*D*), indicating that *egl-36* functions downstream of PKA to inhibit AVL and DVB activation in response to pacemaker. We found that *inx-1* mutations significantly suppressed the expulsion defects of *egl-36(gf)* mutants (Fig. 6*D*) but failed to suppress the expulsion defects caused by *egl-36(gf)* overexpression (Fig. 6*E*), suggesting that *inx-1* mutations suppress the expulsion defects caused by weak but not strong AVL/DVB hyperpolarization. Finally, *egl-36(gf)* mutations completely blocked the ectopic calcium spikes of *inx-1* mutants (Fig. 6*F*). Thus, INX-1 suppresses

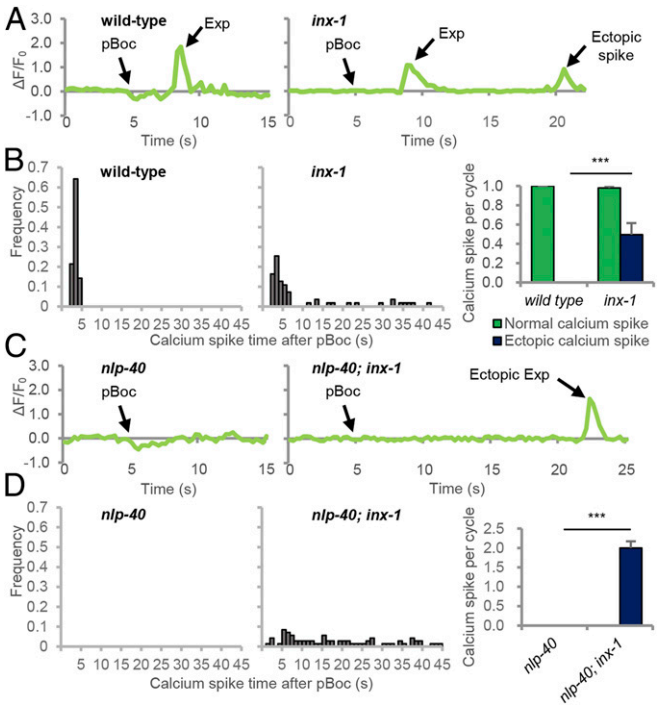

Fig. 5. INX-1 inhibits ectopic activation of the DVB motor neuron. (*A* and *C*) Representative traces showing change of GCaMP3 fluorescence at the AVL/DVB NMJs during the defecation cycle in adult animals of the indicated genotypes expressing GCaMP3 under the *unc-47(mini)* promoter. (*B* and *D*, *Left*) Histograms showing the time when each calcium spike occurred after pBoc in wild-type and *inx-1* mutants. (*Right*) Average frequency of calcium spikes per cycle grouped by normal and ectopic spikes in wild-type and *inx-1* mutants. Means and SEs are shown. Asterisks indicate significant differences: $***P < 0.001$ in Student's *t* test.

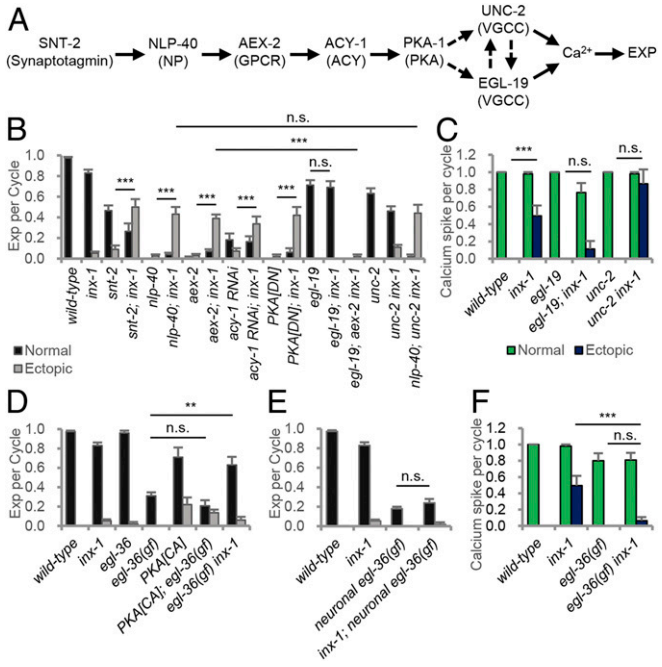

Fig. 6. Ectopic activation of the DVB motor neuron in *inx-1* mutants are suppressed in *egl-19* or *egl-36(gf)* mutants. (*A*) Diagram of the pacemaker controlled signaling pathway that leads to calcium influx at AVL/DVB NMJs and contraction of the enteric muscle (Exp). NP = neuropeptide; ACY = adenylate cyclase. (*B*) Quantification of the number of Exp per defecation cycle in adults of the indicated genotypes. *PKA[DN]* denotes a dominant negative PKA transgene expressed in GABAergic neurons (under the *unc-47* promoter). (*C*) Average frequency of normally timed and ectopic (greater than 5 s) calcium spike per cycle in the indicated mutants. (*D* and *E*) Quantification of the number of Exp per defecation cycle in adults of the indicated genotypes. *PKA[CA]* denotes a constitutively active PKA transgene expressed in GABAergic neurons (under the *unc-47* promoter). Neuronal *egl-36(gf)* denotes *egl-36* (gain-of-function) transgene expressed under the GABAergic *unc-47* promoter. (*F*) Average frequency of normally timed and ectopic (greater than 5 s) calcium spike per cycle in the indicated mutants. Means and SEs are shown. Asterisks indicate significant differences: $***P < 0.001$ and $**P < 0.01$ in Student's *t* test; n.s., not significant.

DVB activation by a mechanism that likely involves membrane hyperpolarization by potassium channels.

Discussion

Here, using a simple circuit that controls a minute time-scale rhythm, we show that electrical synapses coupling a pair of motor neurons coordinates the chemical synaptic output of NMJs to ensure the robust and precise execution of a rhythmic behavior. INX-1/innexin functions in the mature circuit to synchronize the pacemaker-induced activation of AVL and DVB and to also inhibit ectopic activation of DVB during cycle intervals. We propose that by functionally coupling AVL and DVB NMJs, INX-1 promotes synchronized activation of the neurons by mediating lateral excitation of one neuron to the other in response to pacemaker signaling and silences each neuron in between cycles by mediating shunting inhibition when pacemaker signaling is low (Fig. 7). Our results provide a mechanistic understanding of how electrical synapses may fine-tune synaptic output in rhythmic circuits in other organisms.

Prior studies suggest that NLP-40 is rhythmically secreted from the intestine, since the intestine generates calcium waves required for enteric muscle contraction, and NLP-40 secretion is partially dependent upon SNT-2/synaptotagmin, an intestinal calcium sensor for exocytosis. NLP-40 is likely to be predominately secreted from the anterior region of the intestine, whereas AVL and DVB NMJs are located in the posterior of the animal (26, 47). Thus, NLP-40 must diffuse through the body cavity (pseudocoelom) following its secretion over a distance of hundreds of microns. Because NLP-40 functions as a volume transmitter, it is likely to lose temporal precision due to the distance it has to travel before AEX-2/GPCR binding on AVL and DVB. We propose that electrical coupling between the two neurons that respond to NLP-40 has evolved as an effective way of tuning an imprecisely timed analog input (NLP-40) into a precisely timed all-or-none response (calcium transient and GABA release) at NMJs. The role of electrical synapses in synchronizing neuronal activities have been well supported by in vitro studies of mammalian connexins. Spinal motor neurons lacking connexin 40 show temporally uncorrelated firing (48). Connexin 36 knockout leads to asynchronous rhythmic activities between the excitatory neurons of inferior olive (5) and inhibitory neurons of the neocortex (49, 50). A more recent in vivo study of connexin 36 knockout mice showed lack of precise correlated activities in cerebellar Golgi cells (51).

Our results support the idea that a major mechanism by which INX-1 tunes the synchronization of AVL and DVB activity is through mediating lateral excitation from AVL to DVB. We found that under conditions where only AVL was capable of being activated by the pacemaker, AVL could promote the generation of calcium transients in DVB that are dependent on *inx-1* (Fig. 4). In addition, the timing of AVL activation was largely unaffected in animals lacking *inx-1*, whereas DVB activation was late and asynchronous, suggesting that electrical coupling is required for proper timing of DVB activation (Fig. 3). Our results show that synchronized firing of both AVL and DVB also promotes enteric muscle contraction reliably in every cycle. First, ablation of either AVL or DVB reduced expulsion frequency by about half (Fig. 1*B*). Second, calcium imaging of *inx-1* mutants revealed that in cycles in which AVL and DVB activation was asynchronous, expulsion was observed only 42% of the time after the firing of the first or second neuron, and 17% did not show any expulsion either after firing of the first or the second neuron (Fig. 3*E*). In contrast, during the synchronous cycles in *inx-1* mutants, expulsion was always followed by the AVL/DVB calcium spike. Third, the expulsion frequency of *aex-2* mutants in which *aex-2* cDNA was rescued in only AVL was reduced by about half by *inx-1* mutations (from 48 to 22%; Fig. 4), suggesting that activation of AVL alone (in the absence of INX-1) elicits expulsion only half as well as activating AVL and DVB (in the presence of INX-1). Together, these results suggest that the activation and subsequent GABA release from just one neuron has about a 50% probability of promoting enteric muscle contraction, and they underscore the importance of electrical synapse–mediated lateral excitation in increasing reliability of synaptic output. In agreement with this, in mammals, the release of glutamate is shaped by connexin 36–mediated lateral excitation in bipolar cells of the retina (10) and mitral cells of the olfactory bulb (12).

We found that not all lateral excitation between AVL and DVB is mediated by INX-1 since *inx-1* mutations did not eliminate DVB activation by AVL (Fig. 4). The remaining lateral excitation could be explained by two other mechanisms. First, AVL and DVB could be coupled by other innexin proteins. Studies in *C. elegans* using fluorescent reporters for gap junction proteins have shown that AVL and DVB express a number of innexins, including *inx-2*, *inx-10*, *inx-14*, *unc-7*, *unc-9*, *inx-7*, *inx-11*, and *inx-13* (52, 53). Surprisingly, *inx-1* was not reported to be expressed in either AVL or DVB in these studies, suggesting the cis-regulatory elements for expressing *inx-1* may not have been fully covered. Single-cell RNA-sequencing of individual neurons, however, detected *inx-1* expression in both AVL and DVB (54). A prior study reported that INX-1 may form heterotypic gap junctions with INX-10, INX-11, and INX-16 in the *C. elegans*

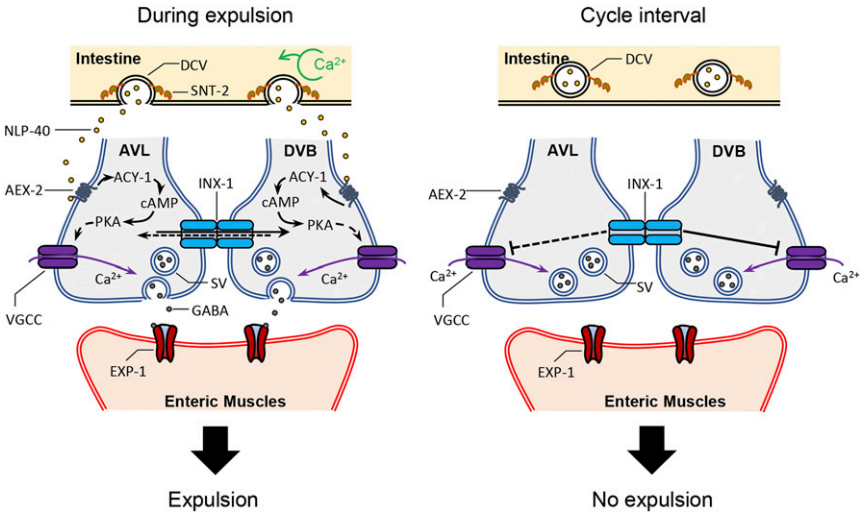

Fig. 7. Working model for INX-1 in the expulsion step of the DMP. (*Left*) During the defecation cycle, calcium oscillation occurs in the intestine around every 50 s. SNT-2 on the DCVs senses the calcium and leads to NLP-40 release from the intestine. NLP-40 activates its receptor, AEX-2, which leads activation of ACY-1 to generate cAMP. Increased cAMP activates PKA, which results in calcium influx to GABAergic motor neurons (AVL and DVB), triggering GABA release. The released GABA activates its receptor, EXP-1, which leads to contraction of enteric muscles (Exp). During NLP-40–induced signaling, INX-1 promotes calcium influx in one neuron in response to activation of the other neuron, leading to synchronized GABA release from both NMJs. (*Right*) During cycle intervals, INX-1 suppresses ectopic activation of the motor neurons by inhibiting ectopic calcium transients. INX-1 sharpens NMJ output by mediating lateral excitation in the presence of signal and shunting inhibition in between cycles when signal is low. Dotted lines are experimentally not shown.

body wall muscle to promote electrical coupling of muscle cells (55). Although we did not identify any other innexins that function as *nlp-40* suppressors, we note that our screening strategy may not have identified innexins that function redundantly with *inx-1* or that were not efficiently knocked down by RNAi, leaving open the possibility that other innexins may function together with INX-1 to regulate expulsion. A second mechanism by which AVL could activate DVB independently of INX-1 could be by ephaptic interaction, which is a nonsynaptic mechanism of activation whereby depolarization of a neuron changes the electrical properties of its surrounding extracellular environments, which in turn affects the excitability of other neurons at the same synaptic region. In vertebrates, ephaptic coupling synchronizes the activity of cortical neurons (56) and mediates the communication between cone and bipolar cells in the retina (57). Once AVL is depolarized at the NMJ by NLP-40 signaling, the local field potential could induce excitability to DVB.

We analyzed two different strains in which only AVL but not DVB could be activated by pacemaker signaling and found that each strain exhibited very different expulsion frequencies. DVB-ablated animals exhibited normally timed expulsions in 63% of cycles (Fig. 1*B*), whereas *aex-2 inx-1* mutants expressing *aex-2* specifically in AVL exhibited a normally timed expulsion in just 22% of cycles (Fig. 4). What accounts for such an apparent discrepancy in expulsion phenotypes in these strains? Prior studies support the idea that the pacemaker controls a GABA-independent signaling pathway since mutants lacking the GABA biosynthetic enzyme UNC-25 or the GABA receptor EXP-1 exhibit less severe expulsion frequency defects than *aex-2* or *nlp-40* mutants (23, 58). Since our rescued *aex-2* mutant strains lack *aex-2* in all neurons except in AVL (and other neurons that are expressed by the *flp-22* promoter), we speculate that the more severe expulsion defects may arise from the disruption of the GABA-independent signaling pathway in these strains. Under normal conditions, GABA provides nearly all of the drive for expulsion, but the importance of the GABA-independent pathway is revealed in animals with compromised GABA signaling (e.g., upon DVB ablation).

Our study also revealed that INX-1 inhibits the activation of DVB during the 50 s interval between cycles when NLP-40 is presumably not released. Live calcium imaging showed that ectopic calcium spikes occurred in DVB at random times in both *inx-1* mutants and *nlp-40; inx-1* double mutants, suggesting that these neurons can be randomly activated even in the absence of pacemaker signaling. The ectopic calcium spikes in *inx-1* mutants were not accompanied by expulsion, whereas the ectopic calcium spikes in *nlp-40*; *inx-1* mutants were generally accompanied by expulsion. Prior studies have suggested the existence of a refractory period during which expulsion cannot take place within a certain time after the preceding expulsion (26, 27), which would explain why the ectopic calcium spikes in *inx-1* mutants did not elicit enteric muscle contraction. We speculate that DVB and AVL may have different electrophysiological properties at rest: DVB is noisier perhaps due to a more depolarized resting potential arising from background leak currents, resulting in an ectopic activation in the absence of INX-1. However, in the presence of INX-1, the ectopic activation is suppressed in DVB by shunting of the background leak currents into AVL. In the backward motor circuit of *C. elegans*, absence of electrical coupling leads to an increase in spontaneous excitatory activity in the premotor interneuron (18). Coupling to AVL could also help to reduce excitability of DVB by decreasing input resistance (18, 49, 59) and/or increasing membrane capacitance (60).

Because the ectopic calcium spikes and enteric muscle contractions in the absence of INX-1 were dependent upon the EGL-19 L-type VGCCs), but not the UNC-2 non-L-type VGCCs, we speculate that the leak currents in DVB may selectively open EGL-19 VGCCs. Indeed, mammalian L-type channels open at lower potentials compared to non-L-type calcium channels (61). Thus, the background leak currents in DVB may induce sufficient voltage change to open EGL-19 channels but not enough to open UNC-2 channels. We found that hyperpolarization of AVL and DVB induced by constitutively active EGL-36 potassium channel mutants also abolished the ectopic calcium spikes in *inx-1* mutants but failed to suppress the pacemaker signaling-induced calcium transients (Fig. 6*F*), suggesting that the leak currents are no longer able to trigger ectopic calcium transients, but pacemaker signaling can promote opening of the calcium channels under these conditions. Thus, during a normal cycle, the large depolarizing currents

generated by NLP-40–mediated activation likely override the currents being dampened by shunting, enabling both neurons to become simultaneously active. Further analysis by electrophysiology will provide a deeper understanding of how electrical synapses coordinate the activities of this neuron pair during this motor program.

Materials and Methods

Strains and Transgenic Lines. Strains were maintained at room temperature on nematode growth media (NGM) plates with OP50 *Escherichia coli* as a food source. The wild-type strain was N2 Bristol. Transgenic lines were generated by injecting into N2 or corresponding mutants with expression plasmids together with coinjection markers KP#708 (*Pttx-3::RFP* at 40 ng/μL) or KP#1338 (*Pttx-3::GFP* at 40 ng/μL) or KP#1106 (*Pmyo-2::NLS::GFP* at 5 ng/μL) or KP#1368 (*Pmyo-2::NLS::mCherry* at 5ng/μL) or pJQ70 (*Pofm-1::mCherry* at 25 ng/μL). Microinjection was performed using standard procedures (62). Generally, three lines were analyzed, and one representative line was used for quantification. Integration of arrays was performed using ultraviolet irradiation as described (63). The strains and transgenic lines used in this study are listed in *SI Appendix*, Table S1.

Molecular Biology. Plasmids were constructed using the backbone pPD49.26 or pPD117.01 (A. Fire, Stanford University School of Medicine, Stanford, CA). Promoter regions were amplified from genomic DNA of *C. elegans* and cDNA were used to clone genes using standard molecular biological techniques. A detailed list of plasmids and oligos are described in *SI Appendix*, Tables S1 and S2.

More detailed materials and methods including information of *nlp-40* suppressor screening, behavioral assays, RNA Interference, fluorescence and calcium live imaging, cell ablation, and histamine chloride inhibition are available in *SI Appendix*.

Data Availability. Reagents generated in this study, including *C. elegans* strains, transgenes, and expression constructs, as well as research protocols will be provided openly to interested investigators upon request. All other study data are included in the article and/or supporting information.

ACKNOWLEDGMENTS. *C. elegans* strains used in this work were provided by the Caenorhabditis Genetics Centre (University of Minnesota), which is funded by NIH Office of Research Infrastructure Programs (P40 OD010440). We thank members of the Sieburth laboratory for discussions and critical reading of the manuscript, the Jim Knowles laboratory for whole genome sequencing, Zhao-Wen Wang for the *inx-1(tm3524)* allele, Oliver Hobert for the *unc-25(Δ)* promoter, William Schafer for the codon-optimized Cx36 plasmid, and David Hall for assisting with gap junction identification in electron micrographs. We also thank John White for sharing the transmission electron micrograph data for animal JSE to the laboratory of David Hall for long-term curation; these data originally came from the MRC/LMB laboratory of Sydney Brenner and can be accessed at https://www.wormimage.org/. This work was supported by the NIH grant NS099414 to D.S.

1. B. W. Connors, Synchrony and so much more: Diverse roles for electrical synapses in neural circuits. *Dev. Neurobiol.* **77**, 610–624 (2017).
2. A. E. Pereda, Electrical synapses and their functional interactions with chemical synapses. *Nat. Rev. Neurosci.* **15**, 250–263 (2014).
3. P. Mann-Metzer, Y. Yarom, Electrotonic coupling interacts with intrinsic properties to generate synchronized activity in cerebellar networks of inhibitory interneurons. *J. Neurosci.* **19**, 3298–3306 (1999).
4. G. P. Dugué *et al*., Electrical coupling mediates tunable low-frequency oscillations and resonance in the cerebellar Golgi cell network. *Neuron* **61**, 126–139 (2009).
5. M. A. Long, M. R. Deans, D. L. Paul, B. W. Connors, Rhythmicity without synchrony in the electrically uncoupled inferior olive. *J. Neurosci.* **22**, 10898–10905 (2002).
6. R. S. Van Der Giessen *et al*., Role of olivary electrical coupling in cerebellar motor learning. *Neuron* **58**, 599–612 (2008).
7. M. L. Veruki, E. Hartveit, AII (Rod) amacrine cells form a network of electrically coupled interneurons in the mammalian retina. *Neuron* **33**, 935–946 (2002).
8. K. Vervaeke, A. Lőrincz, Z. Nusser, R. A. Silver, Gap junctions compensate for sublinear dendritic integration in an inhibitory network. *Science* **335**, 1624–1628 (2012).
9. S. Trenholm *et al*., Nonlinear dendritic integration of electrical and chemical synaptic inputs drives fine-scale correlations. *Nat. Neurosci.* **17**, 1759–1766 (2014).
10. S. P. Kuo, G. W. Schwartz, F. Rieke, Nonlinear spatiotemporal integration by electrical and chemical synapses in the retina. *Neuron* **90**, 320–332 (2016).
11. I. Rabinowitch, W. R. Schafer, "Electrical coupling in Caenorhabditis elegans mechanosensory circuits" in *Network Functions and Plasticity*, J. Jing, Ed. (Academic Press, 2017), chap. 1, pp. 1–11.
12. J. M. Christie, G. L. Westbrook, Lateral excitation within the olfactory bulb. *J. Neurosci.* **26**, 2269–2277 (2006).
13. M. Chatzigeorgiou, W. R. Schafer, Lateral facilitation between primary mechanosensory neurons controls nose touch perception in C. elegans. *Neuron* **70**, 299–309 (2011).
14. P. Alcamí, A. E. Pereda, Beyond plasticity: The dynamic impact of electrical synapses on neural circuits. *Nat. Rev. Neurosci.* **20**, 253–271 (2019).
15. M. V. L. Bennett, R. S. Zukin, Electrical coupling and neuronal synchronization in the Mammalian brain. *Neuron* **41**, 495–511 (2004).
16. J. Hjorth, K. T. Blackwell, J. H. Kotaleski, Gap junctions between striatal fast-spiking interneurons regulate spiking activity and synchronization as a function of cortical activity. *J. Neurosci.* **29**, 5276–5286 (2009).
17. I. Rabinowitch, M. Chatzigeorgiou, W. R. Schafer, A gap junction circuit enhances processing of coincident mechanosensory inputs. *Curr. Biol.* **23**, 963–967 (2013).
18. T. Kawano *et al*., An imbalancing act: Gap junctions reduce the backward motor circuit activity to bias C. elegans for forward locomotion. *Neuron* **72**, 572–586 (2011).
19. D. W. C. Liu, J. H. Thomas, Regulation of a periodic motor program in C. elegans. *J. Neurosci.* **14**, 1953–1962 (1994).
20. P. Dal Santo, M. A. Logan, A. D. Chisholm, E. M. Jorgensen, The inositol trisphosphate receptor regulates a 50-second behavioral rhythm in C. elegans. *Cell* **98**, 757–767 (1999).
21. J. H. Thomas, Genetic analysis of defecation in Caenorhabditis elegans. *Genetics* **124**, 855–872 (1990).
22. S. L. McIntire, E. Jorgensen, J. Kaplan, H. R. Horvitz, The GABAergic nervous system of Caenorhabditis elegans. *Nature* **364**, 337–341 (1993).
23. A. A. Beg, E. M. Jorgensen, EXP-1 is an excitatory GABA-gated cation channel. *Nat. Neurosci.* **6**, 1145–1152 (2003).
24. T. Teramoto, K. Iwasaki, Intestinal calcium waves coordinate a behavioral motor program in C. elegans. *Cell Calcium* **40**, 319–327 (2006).
25. K. Nehrke, J. Denton, W. Mowrey, Intestinal Ca2+ wave dynamics in freely moving C. elegans coordinate execution of a rhythmic motor program. *Am. J. Physiol. Cell Physiol.* **294**, C333–C344 (2008).
26. H. Wang *et al*., Neuropeptide secreted from a pacemaker activates neurons to control a rhythmic behavior. *Curr. Biol.* **23**, 746–754 (2013).
27. T. R. Mahoney *et al*., Intestinal signaling to GABAergic neurons regulates a rhythmic behavior in Caenorhabditis elegans. *Proc. Natl. Acad. Sci. U.S.A.* **105**, 16350–16355 (2008).
28. M. Farrant, Z. Nusser, Variations on an inhibitory theme: Phasic and tonic activation of GABA(A) receptors. *Nat. Rev. Neurosci.* **6**, 215–229 (2005).
29. A. A. Beg, G. G. Ernstrom, P. Nix, M. W. Davis, E. M. Jorgensen, Protons act as a transmitter for muscle contraction in C. elegans. *Cell* **132**, 149–160 (2008).
30. Y. B. Qi, E. J. Garren, X. Shu, R. Y. Tsien, Y. Jin, Photo-inducible cell ablation in Caenorhabditis elegans using the genetically encoded singlet oxygen generating protein miniSOG. *Proc. Natl. Acad. Sci. U.S.A.* **109**, 7499–7504 (2012).
31. S. Xu, A. D. Chisholm, Highly efficient optogenetic cell ablation in C. elegans using membrane-targeted miniSOG. *Sci. Rep.* **6**, 21271 (2016).
32. K. Kim, C. Li, Expression and regulation of an FMRFamide-related neuropeptide gene family in Caenorhabditis elegans. *J. Comp. Neurol.* **475**, 540–550 (2004).
33. J. E. Sulston, Post-embryonic development in the ventral cord of Caenorhabditis elegans. *Philos. Trans. R. Soc. Lond. B Biol. Sci.* **275**, 287–297 (1976).
34. S. L. Rea, D. Wu, J. R. Cypser, J. W. Vaupel, T. E. Johnson, A stress-sensitive reporter predicts longevity in isogenic populations of Caenorhabditis elegans. *Nat. Genet.* **37**, 894–898 (2005).
35. J. G. White, E. Southgate, J. N. Thomson, S. Brenner, The structure of the nervous system of the nematode Caenorhabditis elegans. *Philos. Trans. R. Soc. Lond. B Biol. Sci.* **314**, 1–340 (1986).
36. R. M. Weimer *et al*., UNC-13 and UNC-10/rim localize synaptic vesicles to specific membrane domains. *J. Neurosci.* **26**, 8040–8047 (2006).
37. Y. Goshima, F. Nakamura, P. Strittmatter, S. M. Strittmatter, Collapsin-induced growth cone collapse mediated by an intracellular protein related to UNC-33. *Nature* **376**, 509–514 (1995).
38. T. A. Maniar *et al*., UNC-33 (CRMP) and ankyrin organize microtubules and localize kinesin to polarize axon-dendrite sorting. *Nat. Neurosci.* **15**, 48–56 (2011).
39. K. T. Simonsen, D. G. Moerman, C. C. Naus, Gap junctions in C. elegans. *Front. Physiol.* **5**, 40 (2014).
40. A. Beckmann, A. Grissmer, E. Krause, T. Tschernig, C. Meier, Pannexin-1 channels show distinct morphology and no gap junction characteristics in mammalian cells. *Cell Tissue Res.* **363**, 751–763 (2016).
41. G. E. Sosinsky *et al*., Pannexin channels are not gap junction hemichannels. *Channels* **5**, 193–197 (2011).
42. I. Rabinowitch, M. Chatzigeorgiou, B. Zhao, M. Treinin, W. R. Schafer, Rewiring neural circuits by the insertion of ectopic electrical synapses in transgenic C. elegans. *Nat. Commun.* **5**, 4442 (2014).
43. D. H. Hall, Gap junctions in C. elegans: Their roles in behavior and development. *Dev. Neurobiol.* **77**, 587–596 (2017).
44. N. Pokala, Q. Liu, A. Gordus, C. I. Bargmann, Inducible and titratable silencing of Caenorhabditis elegans neurons in vivo with histamine-gated chloride channels. *Proc. Natl. Acad. Sci. U.S.A.* **111**, 2770–2775 (2014).
45. H. Wang, D. Sieburth, PKA controls calcium influx into motor neurons during a rhythmic behavior. *PLoS Genet.* **9**, e1003831 (2013).
46. D. B. Johnstone, A. Wei, A. Butler, L. Salkoff, J. H. Thomas, Behavioral defects in C. elegans egl-36 mutants result from potassium channels shifted in voltage-dependence of activation. *Neuron* **19**, 151–164 (1997).

47. M. A. Peters, T. Teramoto, J. Q. White, K. Iwasaki, E. M. Jorgensen, A calcium wave mediated by gap junctions coordinates a rhythmic behavior in C. elegans. *Curr. Biol.* **17**, 1601–1608 (2007).
48. K. E. Personius, Q. Chang, G. Z. Mentis, M. J. O'Donovan, R. J. Balice-Gordon, Reduced gap junctional coupling leads to uncorrelated motor neuron firing and precocious neuromuscular synapse elimination. *Proc. Natl. Acad. Sci. U.S.A.* **104**, 11808–11813 (2007).
49. M. R. Deans, J. R. Gibson, C. Sellitto, B. W. Connors, D. L. Paul, Synchronous activity of inhibitory networks in neocortex requires electrical synapses containing connexin36. *Neuron* **31**, 477–485 (2001).
50. M. Blatow *et al*., A novel network of multipolar bursting interneurons generates theta frequency oscillations in neocortex. *Neuron* **38**, 805–817 (2003).
51. I. van Welie, A. Roth, S. S. N. Ho, S. Komai, M. Häusser, Conditional spike transmission mediated by electrical coupling ensures millisecond precision-correlated activity among interneurons In Vivo. *Neuron* **90**, 810–823 (2016).
52. Z. F. Altun, B. Chen, Z.-W. Wang, D. H. Hall, High resolution map of Caenorhabditis elegans gap junction proteins. *Dev. Dynam.* **238**, 1936–1950 (2009).
53. A. Bhattacharya, U. Aghayeva, E. G. Berghoff, O. Hobert, Plasticity of the electrical connectome of C. elegans. *Cell* **176**, 1174–1189.e16 (2019).
54. M. Hammarlund, O. Hobert, D. M. Miller 3rd, N. Sestan, The CeNGEN project: The complete gene expression map of an entire nervous system. *Neuron* **99**, 430–433 (2018).
55. P. Liu *et al*., Six innexins contribute to electrical coupling of C. elegans body-wall muscle. *PLoS One* **8**, e76877 (2013).
56. C. A. Anastassiou, R. Perin, H. Markram, C. Koch, Ephaptic coupling of cortical neurons. *Nat. Neurosci.* **14**, 217–223 (2011).
57. R. Vroman, L. J. Klaassen, M. Kamermans, Ephaptic communication in the vertebrate retina. *Front. Hum. Neurosci.* **7**, 612 (2013).
58. S. L. McIntire, E. Jorgensen, H. R. Horvitz, Genes required for GABA function in Caenorhabditis elegans. *Nature* **364**, 334–337 (1993).
59. T. A. Zolnik, B. W. Connors, Electrical synapses and the development of inhibitory circuits in the thalamus. *J. Physiol.* **594**, 2579–2592 (2016).
60. B. Roerig, M. B. Feller, Neurotransmitters and gap junctions in developing neural circuits. *Brain Res. Brain Res. Rev.* **32**, 86–114 (2000).
61. T. D. Helton, W. Xu, D. Lipscombe, Neuronal L-type calcium channels open quickly and are inhibited slowly. *J. Neurosci.* **25**, 10247–10251 (2005).
62. C. C. Mello, J. M. Kramer, D. Stinchcomb, V. Ambros, Efficient gene transfer in C.elegans: extrachromosomal maintenance and integration of transforming sequences. *The EMBO Journal* **10**, 3959–3970 (1991).
63. M. C. Mariol, L. Walter, S. Bellemin, K. Gieseler, A rapid protocol for integrating extrachromosomal arrays with high transmission rate into the C. elegans genome. *Jove-J. Vis. Exp.* **82**, e50773 (2013).